

# Grid-Forming ( $\lambda - \omega$ ) Virtual Oscillator Control in Converter-Based Power Systems

Taouba Jouini<sup>1</sup>, Emma Tegling<sup>1</sup> and Zhiyong Sun<sup>2</sup>

**Abstract**—Inspired by the kinetics of wave phenomena in reaction-diffusion models of biological systems, we propose a novel grid-forming control strategy for control of three-phase DC/AC converters in power systems. The ( $\lambda - \omega$ ) virtual oscillator control or ( $\lambda - \omega$ ) VOC is a natural increment on ideas from virtual oscillator dynamics rotating at a fixed nominal frequency to adaptive, angle-based frequency function. We study a network of identical three-phase DC/AC converters interconnected via  $\Pi$  transmission lines. For this, we prove almost global asymptotic stability for a reduced (time-scale separated) version of the model, associated to a well-defined set of controller gains and system parameters. Additionally, we link the ( $\lambda - \omega$ ) VOC to well-studied controllers in the literature, e.g. droop control. Finally, we validate our results on an example three DC/AC converter network.

## I. INTRODUCTION

Power generation has always been a major source of air pollution and much effort has been devoted to developing cleaner generation technologies. However, the relatively recent concerns about global warming and sustainability have started to change the way power systems operate and expand and motivated a major shift to renewables with converter-interfaced generation [1]. In the presence of large amounts of converter-interfaced generation, the modeling and design of controllers in power systems needs to be re-thought from new perspectives [2].

*a) Literature:* In essence, the control design for power converters has been driven by two directions of research. On the one hand, the design of oscillators on the circle (or torus), where AC signals are typically assumed to be in quasi-stationary steady state and hence, can be described by their phase angles. The change of the frequency is dictated by the power fluctuations in the grid. This gives rise to droop control [3] and variations thereof [4], which are designed to emulate the dynamics of synchronous machines. Another controller that well translates the advantageous properties of synchronous machines is the matching controller [5] that makes use of available measurements of the voltage deviations of the DC capacitor to *define* the frequency for the electrical grid.

On the other hand, converter control design based on oscillators in rectangular coordinates has also gained attention and is founded on the developed theory of nonlinear oscillations [6]; The Van der Pol oscillator, or more generally Liénard oscillator, gives rise to virtual oscillator control (VOC) in [7], Hopf-like bifurcations inspire dispatchable virtual oscillator (d-VOC) in [8] and alike [9]. Once expressed in polar coordinates after proper time-averaging, virtual oscillator control possesses droop properties that guarantee its compatibility with oscillators on the circle [8], [10] and synchronous machines.

*b) Contributions:* Our contributions in this work are as follows: first, we formulate a control design problem for identical three-phase DC/AC converters whose dynamics are represented by a controllable current source and interconnected via dynamical transmission lines. Motivated by ( $\lambda - \omega$ ) oscillations in biological systems that represent the kinetics of wave phenomena in reaction-diffusion models [11], we propose a grid-forming ( $\lambda - \omega$ ) virtual oscillator control ( $\lambda - \omega$ ) VOC. In particular, given prescribed amplitude and phase angle setpoints, we provide more understanding for the use of phase angles in the control design of DC/AC converters and how it can influence transient stability in converter-based power systems. In particular, we define the system frequency as the *angle difference* relative to desired angle set-point rotating at the frequency of interest. Second, we build upon previously studied virtual oscillator control strategies. Instead of generating sinusoidal waves with a fixed frequency, we introduce an adaptive frequency function based on deviation of phase angles relative to their desired values. By deploying tools from singular perturbation theory, we provide a detailed stability analysis for a reduced model of the closed-loop dynamics. We prove almost global asymptotic stability of the desired steady state set for an explicitly characterized range of system parameters and control gains. Third, we study the properties of the proposed controller and link them to well-studied control strategies, e.g. droop control. Fourth, we corroborate our results through numerical simulations of identical three-phase DC/AC converters in closed-loop with ( $\lambda - \omega$ ) VOC.

Our paper unfurls as follows: Section II presents the setup of the power system model and the overall control objectives. Section III introduces our grid-forming ( $\lambda - \omega$ ) VOC and links it to other control design strategies. Section IV studies the global stability of the desired set of a reduced-order model and identifies parameters and control gains that guarantee stability. Finally, Section V exemplifies our theory via simulations of a three converter system.

\*This work has received funding from the European Research Council (ERC) under the European Union's Horizon 2020 research and innovation program (grant agreement no: 834142) and from the Swedish Research Council under grant 2019-00691.

<sup>1</sup> T. Jouini and E. Tegling are with the Department of Automatic Control, Lund University, Sweden. <sup>2</sup> Z. Sun is with Department of Electrical Engineering, Eindhoven University of Technology, the Netherlands. E-mails: {taouba.jouini, emma.tegling}@control.lth.se, z.sun@tue.nl.

c) *Notation:* We define an undirected graph  $G = (\mathcal{V}, \mathcal{E})$ , where  $\mathcal{V}$  is the set of nodes with  $|\mathcal{V}| = n$  and  $\mathcal{E} \subseteq \mathcal{V} \times \mathcal{V}$  is the set of edges with  $|\mathcal{E}| = m$ . The network topology is specified by the incidence matrix  $\mathcal{B} \in \mathbb{R}^{n \times m}$ . We denote the  $2 \times 2$  identity matrix by  $I_2 = \begin{bmatrix} 1 & 0 \\ 0 & 1 \end{bmatrix}$  and the identity matrix of appropriate dimensions  $p \in \mathbb{N}$  by  $\mathcal{I}$ . We define  $\mathcal{J} = \mathcal{I} \otimes J_2$  with  $J_2 = \begin{bmatrix} 0 & -1 \\ 1 & 0 \end{bmatrix}$ . Let  $\mathbb{S}^1$  define the unit circle. For  $\gamma \in \mathbb{S}^1$ , we define the transformation matrix by  $R(\gamma) = \begin{bmatrix} \cos(\gamma) & \sin(\gamma) \\ -\sin(\gamma) & \cos(\gamma) \end{bmatrix}$ , and  $\mathcal{R}(\gamma) = \mathcal{I} \otimes R(\gamma)$ . Let  $\mathbf{1}_n$  be  $n$ -dimensional vector with all entries being one. Given a set  $\mathcal{A}$ , we denote by  $\|x\|_{\mathcal{A}} = \inf_{a \in \mathcal{A}} d(x, a)$  the distance from a vector  $x \in \mathbb{R}^n$  to the set  $\mathcal{A}$ , where  $d(\cdot, \cdot)$  is a distance metric. Given a dynamical system  $\dot{x} = f(x)$ , we denote by  $x(t, x_0)$  its trajectory at times  $t > 0$  starting at  $x(0) = x_0$ . Given a matrix  $M$ , we denote by  $\|M\|$  its 2-norm, and given a symmetric matrix  $A$ , we denote by  $\lambda_{\min}(A)$  and  $\lambda_2(A)$  its smallest and its second-smallest eigenvalue, respectively.

## II. CONTROL OBJECTIVES

### A. Network model

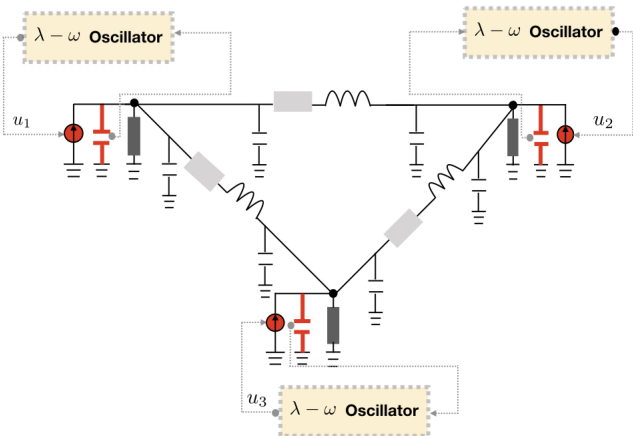


Fig. 1. Power system setup under consideration

Consider a power system model as shown in Figure 1 consisting of averaged and balanced three-phase DC/AC converters and connected via  $\Pi$  transmission lines. Each line consists of a resistance  $R_O > 0$  and an inductance  $L_O > 0$  connected to a shunt capacitor with  $C_O > 0$ . Each DC/AC converter is represented by a controllable current source set in parallel with an output capacitor. This is lumped with line capacitance into  $C > 0$  and connected to a resistive load with conductance  $G > 0$ . The dynamics of the power system model can be described in the  $\alpha\beta$ -frame as follows,

$$\begin{aligned} C \dot{v}_c &= -G v_c - \mathbf{B} i_O + u, \\ L_O \dot{i}_O &= -R_O i_O + \mathbf{B}^\top v_c, \end{aligned} \quad (1)$$

where  $i_O = [i_{O,1}^\top, \dots, i_{O,m}^\top]^\top \in \mathbb{R}^{2m}$  is the line current and  $v_c = [v_{c,1}^\top, \dots, v_{c,n}^\top]^\top \in \mathbb{R}^{2n}$  is the output capacitor voltage. We denote by  $\mathbf{B} = I_2 \otimes \mathcal{B}$  the extended incidence matrix. Let  $u = [u_1^\top, \dots, u_n^\top]^\top \in \mathbb{R}^{2n}$  be a controllable current source

that represents our main control input to be designed in the sequel. For an input  $u_k \in \mathbb{R}^2$ , we denote its polar coordinates by  $[r_k, \theta_k]^\top$ , where  $u_{\alpha,k} = r_k \cos(\theta_k)$ ,  $u_{\beta,k} = r_k \sin(\theta_k)$ , as well as  $r = [r_1, \dots, r_n]^\top$  and  $\theta = [\theta_1, \dots, \theta_n]^\top$ .

### B. Control objectives

We increment (1) as follows,

$$\begin{aligned} u &= \mathcal{F}(u(s), \hat{y}(s), 0 \leq s \leq t), \\ C \dot{v}_c &= -G v_c - \mathbf{B} i_O + u, \\ L_O \dot{i}_O &= -R_O i_O + \mathbf{B}^\top v_c, \end{aligned} \quad (2)$$

where  $\mathcal{F}$  is an operator and  $\hat{y}$  is the output measurement that will be specified in the sequel.

Let  $N$  denote the dimension of the closed-loop system (2),  $\omega^*$  a desired steady state frequency and define  $x = [u^\top, v_c^\top, i_O^\top]^\top$ . Given prescribed amplitudes  $r^* = [r_1^*, \dots, r_n^*]^\top$  and phase angles  $\theta^* = [\theta_1^*, \dots, \theta_n^*]^\top$ , we use the measurement  $\hat{y}$  to design the control input  $u$ . This is achieved by designing the operator  $\mathcal{F}$  as a dynamical oscillator  $\dot{u} = f(u, \hat{y})$  with vector field  $f(u, \hat{y}) = [f_1(u_1, \hat{y}_1), \dots, f_n(u_n, \hat{y}_n)]^\top$  that induces sinusoidal waves at a desired amplitude  $r^*$  and a desired angle  $\theta^* = \omega^* t + \theta_0^*$ ,  $\{\theta_0^* \in \mathbb{S}^1\}$ . In particular, we design the input  $u$  to stabilize (2) at a desired synchronous steady state set described by,

$$\mathcal{S} = \{x \in \mathbb{R}^N, x = x^*\},$$

whereby,

$$\mathcal{S}_u = \left\{ u \in \mathbb{R}^{2n}, [r^\top, \theta^\top]^\top = [r^{*\top}, \theta^{*\top}]^\top, \dot{\theta}^* = \omega^* \mathbf{1}_n \right\}.$$

Note that the steady state values of  $x^*$  are induced by the desired magnitude and phase angle of  $[r^{*\top}, \theta^{*\top}]^\top$ . The sets  $\mathcal{S}$  and  $\mathcal{S}_u$  are frequency synchronous and  $2\pi$ -periodic.

## III. GRID-FORMING ( $\lambda - \omega$ ) VOC

### A. Control design

Our control goal is to sustain AC oscillations at specified amplitude  $r^*$  and phase angle  $\theta^*$ . For this, we propose the nonlinear dynamics inspired by  $(\lambda - \omega)$  systems representing the kinetics of wave phenomena in reaction-diffusion models of biological systems [11],

$$f_k := \begin{bmatrix} -\lambda_k(r_k, r_k^*) & \tilde{\omega}_k(\theta_k, \theta_k^*) \\ -\tilde{\omega}_k(\theta_k, \theta_k^*) & -\lambda_k(r_k, r_k^*) \end{bmatrix} u_k + \tilde{h}_k(v_{c,k}).$$

Here  $u_k$  is the input and  $u_k^*$  is a given reference in polar coordinates  $[r_k^*, \theta_k^*]^\top$  and we have set  $\hat{y}_k = v_{c,k}$ . The function  $\tilde{h}_k(\cdot)$  depends explicitly on the local output voltage measurement  $v_{c,k}$ , whose reference  $v_{c,k}^*$  is assumed to be available. We introduce the following amplitude function,

$$\lambda_k(r_k, r_k^*) = \gamma_k \left( \frac{r_k}{r_k^*} - 1 \right), \quad (3)$$

as well as the frequency function,

$$\tilde{\omega}_k(\theta_k, \theta_k^*) = \alpha_k(\theta_k - \theta_k^*) - \omega^*, \quad \alpha_k > 0, \quad (4)$$

where  $\gamma_k$  and  $\alpha_k$  are positive control gains and  $\theta \in [0, 2\pi)$ . Note that, the frequency function (4) is a novelty in our

work in comparison to other suggestions of virtual oscillator control. For a discussion, see Section III-B.

If  $\tilde{h}_k(v_{c,k}) = 0$ , then the  $(\lambda - \omega)$  VOC dynamics can be expressed compactly in polar coordinates, as follows

$$\begin{bmatrix} \dot{r}_k \\ \dot{\theta}_k \end{bmatrix} = \begin{bmatrix} -r_k \lambda_k(r_k, r_k^*) \\ -\tilde{\omega}_k(\theta_k, \theta_k^*) \end{bmatrix}. \quad (5)$$

Next, we design

$$\tilde{h}_k(v_{c,k}, v_{c,k}^*) = \Pi_k v_{c,k}, \quad \Pi_k = \mathbf{I}_2 - \frac{v_{c,k}^* v_{c,k}^{*\top}}{v_{c,k}^{*\top} v_{c,k}^*}.$$

Note that, for  $r_k = r_k^*$  and  $\theta_k = \theta_k^*$ , the  $(\lambda - \omega)$  VOC is a harmonic oscillator rotating at the desired frequency  $\omega^*$ .

By defining,

$$\begin{aligned} \tilde{K}(\theta, \theta^*) &= \mathcal{I} \otimes (\mathbf{J}_2 \tilde{\omega}_k(\theta_k, \theta_k^*)), \\ \Lambda(r, r^*) &= \mathcal{I} \otimes (\mathbf{I}_2 \lambda_k(r_k, r_k^*)), \\ \Pi_c &= \text{diag}(\Pi_1, \dots, \Pi_n), \end{aligned}$$

the closed-loop system becomes,

$$\dot{u} = -\left(\Lambda(r, r^*) + \tilde{K}(\theta, \theta^*)\right)u - \Pi_c v_c, \quad (6a)$$

$$C \dot{v}_c = -G v_c - \mathbf{B} i_O + u, \quad (6b)$$

$$L_O \dot{i}_O = -R_O i_O + \mathbf{B}^\top v_c. \quad (6c)$$

A summarizing diagram of the overall closed-loop system is presented in Figure 2.

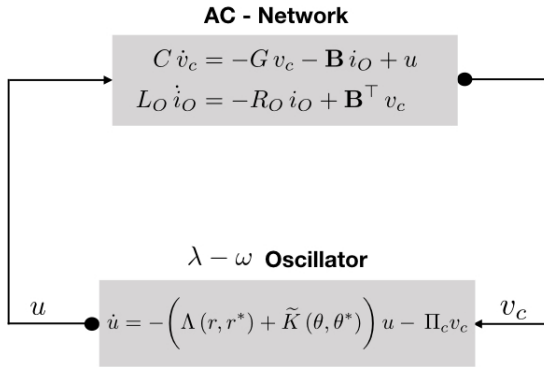


Fig. 2. Summarizing diagram of  $(\lambda - \omega)$  VOC.

### B. Interpretation of grid-forming $(\lambda - \omega)$ VOC

By design, the  $(\lambda - \omega)$  virtual oscillator in (6) is a grid-forming converter in the sense of [12].

a) *Droop control*: Droop control is a well-studied control strategy both in theory and practice. For this reason, it is regarded as a compass for evaluating the performance of novel control strategies as well as their compatibility with other controllers (with droop behavior) and synchronous machines.

**Proposition III.1.** Consider the grid-forming  $(\lambda - \omega)$  VOC in (6). Define

$$P_k = u_k^\top v_{c,k}, \quad P_{ref,k} = u_k^\top \frac{v_{c,k}^* v_{c,k}^{*\top}}{v_{c,k}^{*\top} v_{c,k}^*} v_{c,k},$$

$$Q_k = u_k^\top \mathbf{J}_2 v_{c,k}, \quad Q_{ref,k} = u_k^\top \mathbf{J}_2 \frac{v_{c,k}^* v_{c,k}^{*\top}}{v_{c,k}^{*\top} v_{c,k}^*} v_{c,k}.$$

Then, the  $(\lambda - \omega)$  VOC has a droop-like behavior given by the following equations,

$$\dot{r}_k = -\gamma_k r_k \left( \frac{r_k}{r_k^*} - 1 \right) + \frac{-P_k + P_{ref,k}}{r_k}, \quad (7a)$$

$$\dot{\theta}_k = \omega_0 - \alpha_k (\theta_k - \theta_k^*) + \frac{-Q_k + Q_{ref,k}}{r_k}. \quad (7b)$$

*Proof.* From equation (6a), we use the relationship  $r_k = \sqrt{u_k^\top u_k}$  and calculate

$$\begin{aligned} \dot{r}_k &= \frac{1}{2r_k} (u_k^\top \dot{u}_k + \dot{u}_k^\top u_k) \\ &= \frac{1}{r_k} u_k^\top (-[\lambda(r_k, r_k^*) \mathbf{I}_2 + \mathbf{J}_2 \omega_k(\theta_k, \theta_k^*)] u_k - \Pi_c v_c), \end{aligned}$$

which together with the definition of  $P_k$  amounts to (7a).

For the second statement, we define  $u_k = r_k [\sin(\theta_k) \cos(\theta_k)]^\top$ . Its time derivative is given by  $\dot{u}_k = \dot{r}_k [\sin(\theta_k) \cos(\theta_k)]^\top + \dot{\theta}_k r_k \mathbf{J}_2 [\sin(\theta_k) \cos(\theta_k)]^\top$ . We multiply from the left by  $u_k^\top \mathbf{J}_2^\top$  to obtain

$$\dot{\theta}_k = \frac{-1}{r_k} [\sin(\theta_k) \cos(\theta_k)] \mathbf{J}_2 \dot{u}_k.$$

By substituting  $\dot{u}_k$  as given in (6a), this amounts to (7b).  $\square$

Around the nominal frequency and amplitude, in addition to the active power to amplitude, or  $(P - r)$  droop, the adaptive frequency in (4) introduces a droop behavior (7b) between the reactive power and the phase angle deviations, or  $(Q - \theta)$  droop.

b) *Van-der-Pol/Liénard Oscillator*: The virtual oscillator control was initially proposed in [13] based on the implementation of Van Der Pol Oscillator, or Liénard-oscillator in general. The Liénard Oscillator is the sum of a linear harmonic oscillator with an additional non-linearity implemented electrically as a nonlinear voltage-dependent current source. In the proposed oscillator, the non-linearity in  $(\lambda - \omega)$  oscillator is instead in the amplitude (dependent on the input magnitude) as well as the frequency (dependent on the phase angle) functions.

c) *Hopf-like Oscillators:*

- 1) *Dispatchable-VOC (d-VOC)* The dispatchable virtual oscillator control follows by design the normal-form of Hopf bifurcation [8]. The  $(\lambda - \omega)$  VOC links structurally to the amplitude control in d-VOC.
- 2) *Andronov Hopf Oscillator* Another variation of Hopf oscillators is the Andronov Hopf Oscillator proposed in [9], [14]. This is the same as d-VOC except for an amplitude function squared in its arguments.

The main novelty of  $(\lambda - \omega)$  VOC in comparison to d-VOC/Andronov Hopf is the design of an adaptive frequency function via  $\omega_k(\cdot, \cdot)$  based on phase angle deviations relative to nominal.

d) *Matching control:* The matching control can be interpreted as a virtual oscillator with a feedback-based frequency function that exploits DC measurements (see Fig. 2 in [15]) but without an amplitude regulation function. In general, the frequency function is a degree of freedom in the design of  $(\lambda - \omega)$  VOC and can be incremented with a feedback term as in the matching control of the form

$$\omega(v_{dc}, v_{dc}^*, \theta, \theta^*) = \eta(v_{dc} - v_{dc}^*) - \alpha(\theta - \theta^*),$$

where  $v_{dc}$  is the DC capacitor voltage and  $v_{dc}^*$  the nominal DC voltage.

#### IV. STABILITY ANALYSIS

We transform the overall closed-loop system into the  $dq$ -frame rotating at  $\theta_{dq}(t) = \omega^* t$  as follows:

$$i_{dq} = \mathcal{R}(\omega^* t) i_O, v_{dq} = \mathcal{R}(\omega^* t) v_C, u_{dq} = \mathcal{R}(\omega^* t) u,$$

where  $\mathcal{R}(\omega^* t)$  is a rotation matrix. The overall closed-loop dynamics can be written in rotating  $dq$ -frame as,

$$\begin{aligned} \dot{u}_{dq} &= -(\Lambda(r, r^*) + K(\theta, \theta^*)) u_{dq} - \Pi_{dq} v_{dq}, \\ C \dot{v}_{dq} &= -Z_G v_{dq} - \mathbf{B} v_{dq} + u_{dq}, \\ L_O \dot{i}_{dq} &= -Z_O i_{dq} + \mathbf{B}^\top v_{dq}, \end{aligned} \quad (8)$$

where  $\Lambda(r, r^*)$  is the amplitude function in (6) and  $K(\theta, \theta^*) = \mathcal{I} \otimes (J_2 \omega_k(\theta_k, \theta_k^*))$  with  $\omega(\theta_k, \theta_k^*) = \alpha_k(\theta_k - \theta_k^*)$ . Furthermore, we define  $Z_G = G\mathcal{I} + C\mathcal{J}\omega^*$  and  $Z_O = R_O\mathcal{I} + L_O\mathcal{J}\omega^*$  as well as  $\Pi_{dq} = \mathcal{I} - \frac{v_{dq}^* v_{dq}^{\top}}{v_{dq}^* v_{dq}^*}$ .

The dynamics (8) satisfy the following steady state equations in the rotating frame,

$$\begin{aligned} 0 &= -(\Lambda(r^*, r^*) + K(\theta^*, \theta^*)) u_{dq}^*, \\ 0 &= -Z_G v_{dq}^* - \mathbf{B} v_{dq}^* + u_{dq}^*, \\ 0 &= -Z_O i_{dq}^* + \mathbf{B}^\top v_{dq}^*, \end{aligned} \quad (9)$$

Note that  $-(\Lambda(r^*, r^*) + K(\theta^*, \theta^*)) u_{dq}^* = 0$  for  $u_{dq}^* = 0$ , or  $r = r^*, \theta = \theta^*$ . To see that the origin is also a solution to the steady state equations (9), note that the remaining states satisfy the following equations with a full rank matrix.

$$\begin{bmatrix} -Z_O & \mathbf{B}^\top \\ -\mathbf{B} & -Z_G \end{bmatrix} \begin{bmatrix} i_{dq}^* \\ v_{dq}^* \end{bmatrix} = \begin{bmatrix} 0 \\ 0 \end{bmatrix}, \quad (10)$$

Next, we make the following assumption,

**Assumption 1.** Let  $\tau^* > 0$  be sufficiently small. Assume that,

$$\frac{L_O}{\sqrt{L_O^2 \omega^{*2} + R_O^2}} < \tau^*. \quad (11)$$

Under Assumption 1, we can avail ourselves of singular perturbation theory for the stability analysis. For this, we write the dynamical system (8) as two coupled subsystems  $\Sigma_1$  and  $\Sigma_2$ . The system dynamics can be described by the following set of differential algebraic equations,

$$\begin{aligned} \Sigma_1 : \dot{u}_{dq} &= -(\Lambda(r, r^*) + K(\theta, \theta^*)) u_{dq} - \Pi_{dq} v_{dq}, \\ \Sigma_2 : C \dot{v}_{dq} &= -Z_G v_{dq} - \mathbf{B} v_{dq} + u_{dq}, \\ 0 &= -Z_O i_{dq} + \mathbf{B}^\top v_{dq}, \end{aligned}$$

where the algebraic equation is considered as limit of the fast dynamics of the boundary-layer system with  $y' = i_{dq} - i_{dq}^*$ , where  $i_{dq}^*$  solves the algebraic equation of  $\Sigma_2$ . Furthermore, the boundary-layer system reads as,

$$\begin{aligned} y' &= -Z_O (y' + Z_O^{-1} \mathbf{B}^\top v_{dq}) + \mathbf{B}^\top v_{dq} \\ &= -Z_O y'. \end{aligned} \quad (12)$$

The origin of (12) is exponentially stable (because  $-Z_O$  is Hurwitz). Thus, the reduced system is defined by,

$$\Sigma_1 : \dot{u}_{dq} = -(\Lambda(r, r^*) + K(\theta, \theta^*)) u_{dq} - \Pi_{dq} v_{dq}, \quad (13a)$$

$$\Sigma_2 : C \dot{v}_{dq} = -L v_{dq} + u_{dq}, \quad (13b)$$

with the impedance matrix  $L = Z_G + \mathbf{B} Z_O^{-1} \mathbf{B}^\top$ .

Theorem 11.1 in [16] can be applied to show that the difference of solution trajectories between the original (8) and reduced system (13) is of the order of  $\mathcal{O}\left(L_O / \sqrt{L_O^2 \omega^{*2} + R_O^2}\right)$  for finite time intervals.

Next, let  $\mathcal{S}'$  denote the steady state set resulting from setting (13) to zero. In the sequel, we study almost global stability of  $\mathcal{S}'$  for any trajectory of (13). We study stability with respect to sets in the sense of Theorem 2.8 in [17]. We refer the interested reader for details therein.

Define  $\xi_2 = \lambda_{\min}(L + L^\top)$ ,  $\beta_1 = 1$ ,  $\beta_2 = \|L^{-1}\|^2 + \gamma_{\max} \|L^{-1}\|$ ,  $\zeta = \|L^{-1}\|$  and  $\gamma_{\max} = \max\{\gamma_1, \dots, \gamma_n\}$ .

Consider the following condition.

**Condition IV.1.** For a sufficiently small  $\alpha^* > 0$  and a constant  $\xi_1 > 0$ , assume that,

$$\max\{\alpha_1, \dots, \alpha_n\} < \alpha^*, \quad (14a)$$

$$\Pi(\gamma_{\max} - \Pi_{dq} L^{-1}) + (\gamma_{\max} - \Pi_{dq} L^{-1})^\top \Pi < -\xi_1 \Pi, \quad (14b)$$

$$\frac{C}{\sqrt{C^2 \omega^{*2} + G^2}} < \frac{\xi_1 \xi_2}{\xi_1 \zeta + \beta_1 \beta_2}, \quad (14c)$$

We state the main result in the following theorem.

**Theorem IV.2.** Consider the system (13) under Condition IV.1. The steady state set  $\mathcal{S}'$  is almost globally asymptotically stable for any trajectory of (13).

Inspired by [8], [18], we prove Theorem IV.2 by proposing the following road map:

- Step 1: Consider the reduced system described by,

$$\dot{u}_{dq} = -(\Lambda(r, r^*) + K(\theta, \theta^*) + \Pi_{dq} L^{-1}) u_{dq}. \quad (15)$$

This step aims to prove the following Proposition.

**Proposition IV.3.** *Consider the reduced system (15). Under Condition IV.1, the steady state set  $\mathcal{S}'_u$  of (15) is almost globally asymptotically stable for any trajectory of (15).*

- Show that  $\mathcal{S}'_{uu} = \text{span}\{u_{dq}^*\}$ ,  $u_{dq}^* \in \mathcal{S}'_u$  is exponentially stable using  $\mathcal{V}_1(u_{dq})$  for any trajectory of (15).
- Show that the origin is an unstable equilibrium with a region of attraction  $\mathcal{S}_0$  of measure zero. See later Lemma IV.4.
- For all initial conditions  $u \in \mathcal{S}'_{uu} \setminus \{0\}$ , show that the set  $\{u_{dq} \in \mathbb{R}^{2n} \mid r = r^*\}$  is asymptotically stable, based on LaSalle invariance principle.

This concludes asymptotic stability of  $\mathcal{S}'_u = \mathcal{S}'_{uu} \cap \{u_{dq} \in \mathbb{R}^{2n} \mid r = r^*\}$  for all trajectories of (15), except those with initial condition on  $\mathcal{S}_0$ . For an illustration of the proof steps, see Figure 3.

- Step 2: We now show the main Theorem IV.2, following singular perturbation ideas from Ch.11.5 of [19]:

- By treating  $u_{dq} \in \mathcal{S}'_u$  as a fixed parameter, show that  $v_{dq}^* = L^{-1} u_{dq}^*$  is exponentially stable using  $\mathcal{V}_2(y)$  as Lyapunov function with  $y = v_{dq} - L^{-1} u_{dq}$  for any trajectory of the boundary-layer system

$$\dot{y} = -L(y + L^{-1} u_{dq}) + u_{dq} = -Ly. \quad (16)$$

- Use Steps 1 and 2 to show asymptotic stability of  $\mathcal{S}'$  using the Lyapunov function  $\mathcal{W}(u_{dq}, y) = (1 - d)\mathcal{V}_1(u_{dq}) + d\mathcal{V}_2(y)$ , with  $0 < d < 1$  with no particular assumptions on  $u_{dq}$  and  $y$ .

*a) Step 1:* Our goal is to investigate the stability of the subspace  $\mathcal{S}'_{uu} = \text{span}\{u_{dq}^*\}$  with  $u_{dq}^* \in \mathcal{S}'_u$ . In the sequel, we take  $h(u_{dq}) = L^{-1} u_{dq}$  and consider the reduced system (15)

We have the following lemma,

**Lemma IV.4.** *Consider the system in (15). The set*

$$\mathcal{S}_0 = \{u_0 \in \mathbb{R}^{2n} : \lim_{t \rightarrow \infty} u_{dq}(t, u_0) = 0\}, \quad (17)$$

*has zero Lesbegue measure and the origin is unstable.*

*Proof.* We inspect the Jacobian of (15) given by,

$$\frac{\partial f}{\partial u_{dq}} \Big|_{u_{dq}=0} = \lim_{u_{dq} \rightarrow 0} (-\Lambda(r, r^*) - K(\theta, \theta^*) - \Pi_{dq} L^{-1}). \quad (18)$$

Note that the first two terms read, for all  $k = 1, \dots, n$  as,

$$\begin{aligned} & \lim_{u_{dq,k} \rightarrow 0} -\lambda_k(r_k, r_k^*) I_2 - \omega_k(\theta_k, \theta_k^*) J_2 \\ &= \lim_{u_{dq,k} \rightarrow 0} -\gamma_k \left( \frac{\sqrt{u_{dq,k}^\top u_{dq,k}}}{r_k^*} - 1 \right) I_2 - \alpha_k(\theta_k - \theta_k^*) J_2 \\ &= \gamma_k \cdot I_2 + \alpha_k \theta_k^* J_2 =: A_k. \end{aligned}$$

The symmetric part of  $A_k$  is positive definite. Hence, for any vector  $v_{dq}^*$ ,  $v_{dq}^{*\top} (\text{diag}(A_1, \dots, A_n) - \Pi_{dq} L^{-1}) v_{dq}^* = v_{dq}^{*\top} \text{diag}(A_1, \dots, A_n) v_{dq}^* > 0$ . This shows that (18) has at least two eigenvalues with positive real part and the origin is unstable. By applying Prop. 11 in [20], we conclude that the set  $\mathcal{S}_0$  given in (17) has measure zero.  $\square$

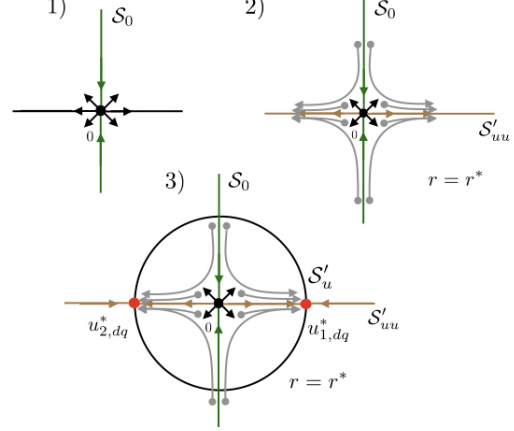


Fig. 3. Sketch of Step 1 in the proof. The set  $\mathcal{S}_0$  is denoted by the vertical green line. The set  $\mathcal{S}'_{uu}$  is represented by the horizontal brown line and the set  $\mathcal{S}'_u$  is denoted by the red dots.

We use as Lyapunov function an projector onto the orthogonal complement of  $u_{dq}^*$  as follows,

$$\mathcal{V}_1(u_{dq}) = u_{dq}^\top \Pi u_{dq}, \quad \Pi = \mathcal{I} - \frac{u_{dq}^* u_{dq}^{*\top}}{u_{dq}^{*\top} u_{dq}^*}. \quad (19)$$

For this, we calculate,

$$\begin{aligned} \dot{\mathcal{V}}_1(u_{dq}) &= -2u_{dq}^\top \Pi ((\Lambda(r, r^*) + K(\theta, \theta^*) + \Pi_{dq} L^{-1}) u_{dq}) \\ &\leq -2u_{dq}^\top \Pi \Pi_{dq} L^{-1} u_{dq} + 2u_{dq}^\top \Pi \Gamma u_{dq} \\ &\leq 2u_{dq}^\top \Pi (\Gamma - \Pi_{dq} L^{-1}) u_{dq} \leq 2u_{dq}^\top \Pi (\gamma_{\max} \mathcal{I} - \Pi_{dq} L^{-1}) u_{dq}, \end{aligned}$$

where  $\Gamma = \text{diag}\{\gamma_1 I_2, \dots, \gamma_n I_2\}$ ,  $\gamma_{\max} = \max\{\gamma_1, \dots, \gamma_n\}$ , and under Condition (14a), it holds that,

$$\begin{aligned} & -(\Pi(\Lambda(r, r^*) + K(\theta, \theta^*)) + (\Lambda(r, r^*) + K(\theta, \theta^*))^\top \Pi) \\ & \leq \Pi \Gamma + \Gamma^\top \Pi. \end{aligned}$$

The details of the calculations are in the Appendix VI.

By choosing  $\gamma_{\max}$ , so that (14b) is satisfied, we have that,

$$u_{dq}^\top \Pi (\gamma_{\max} \mathcal{I} - \Pi_{dq} L^{-1}) u_{dq} \leq -u_{dq}^\top \Pi \xi_1 u_{dq}.$$

Lie derivative is hence negative definite with respect to  $\mathcal{S}'_{uu}$ . This shows that  $\mathcal{S}'_{uu}$  is exponentially stable.

Given the amplitude and angle functions (3), (4), our remaining goal in this step is to show that  $u_{dq}$  converges to the steady state values of the amplitudes on  $\mathcal{S}'_u$ . For this, we introduce the following Lyapunov function,

$$\mathcal{Z}(r) = \frac{1}{2} \sum_{k=1}^n \left(1 - \frac{r_k}{r_k^*}\right)^2,$$

whose Lie derivative is given by,

$$\begin{aligned}\dot{\mathcal{Z}}(r) &= \sum_{k=1}^n \left(1 - \frac{r_k}{r_k^*}\right) \dot{r}_k \\ &= \sum_{k=1}^n -\gamma_k \left(1 - \frac{r_k}{r_k^*}\right)^2 r_k - u_{dq}^\top C \Pi_{dq} L^{-1} u_{dq},\end{aligned}$$

where  $C = \text{diag}\{\frac{1}{r_1}(1 - \frac{r_1}{r_1^*}), \dots, \frac{1}{r_n}(1 - \frac{r_n}{r_n^*})\}$ . From the previous step, we know that  $\mathcal{S}'_{uu}$  is exponentially stable. This implies that  $L^{-1}u_{dq} \rightarrow L^{-1}\text{span}\{u_{dq}^*\} = \text{span}\{v_{dq}^*\}$  and hence  $\lim_{t \rightarrow \infty} \|\Pi_{dq} L^{-1} u_{dq}(t)\| \rightarrow 0$ . From  $\|\Pi_{dq} L^{-1} u_{dq}(t)\| \leq \|\Pi_{dq} L^{-1} u_{dq}(0)\|$  and by setting  $\|\Pi_{dq} L^{-1} u_{dq}(0)\| = 0$ , we have,

$$\dot{\mathcal{Z}}(r) \leq -\sum_{k=1}^n \gamma_k \left(1 - \frac{r_k}{r_k^*}\right)^2 r_k.$$

Note that by  $u_{dq} \neq 0$ , it holds that  $r_k > 0$ . Since the sub-level sets of  $\mathcal{Z}(r)$  are compact, the trajectories of (13) starting on  $\Omega_{c_0}(u_{dq}) = \{\mathcal{Z}(r) \leq c_0\}$  are bounded. We invoke LaSalle invariance principle to deduce asymptotic stability of the set  $\mathcal{S}'_u$  for all trajectories starting from  $\mathcal{S}'_{uu}$ .

Hereby, we infer almost global stability of the desired steady state set  $\mathcal{S}'_u = \{u_{dq} \in \mathbb{R}^{2n} | r = r^*\} \cap \mathcal{S}'_{uu}$  and conclude the proof of Proposition IV.3.

b) *Step 2:* In this step, consider the boundary-layer system given by (16). Since  $-L$  is Hurwitz, the origin is exponentially stable for all trajectories of the boundary-layer system (16) with the Lyapunov function  $\mathcal{V}_2 = \frac{1}{2}y^\top y$ .

Next, we consider the convex combination

$$\mathcal{W}(u_{dq}, v_{dq}) = (1-d)\mathcal{V}(u_{dq}) + d\mathcal{V}_2(y).$$

By taking the derivative,

$$\begin{aligned}\dot{\mathcal{W}}(u_{dq}, v_{dq}) &= (1-d)\dot{\mathcal{V}}(u_{dq}) + 2dy^\top \dot{y} \\ &= 2(1-d)u_{dq}^\top \Pi(-(\Lambda(r, r^*) + K(\theta, \theta^*))u_{dq} \\ &\quad - \Pi_{dq}(y + L^{-1}u_{dq})) + 2\frac{d}{\varepsilon}y^\top (-Ly) \\ &\quad - 2dy^\top L^{-\top}(-(\Lambda(r, r^*) + K(\theta, \theta^*))u_{dq} - \Pi_{dq}(y + L^{-1}u_{dq})).\end{aligned}$$

For the mixed terms in  $u_{dq}$  and  $y$ , we calculate

$$\begin{aligned}y^\top L^{-\top} [(\Lambda(r, r^*) + K(\theta, \theta^*))u_{dq} + \Pi_{dq}(y + L^{-1}u_{dq})] &\leq \\ \|y\| (\|L^{-\top} \Pi_{dq} L^{-1}\| + \gamma_{\max} \|L^{-\top}\|) \|u_{dq}\|_{\mathcal{S}'_u} + \|y\|^2 \|L^{-\top} \Pi_{dq}\| &\leq \\ \|y\| (\|L^{-1}\|^2 + \gamma_{\max} \|L^{-1}\|) \|u_{dq}\|_{\mathcal{S}'_u} + \|y\|^2 \|L^{-1}\|, &\end{aligned}$$

as well as the inequality  $-u_{dq}^\top \Pi_{dq} y \leq \|u_{dq}\|_{\mathcal{S}'_u} \|y\|$ . By condition (14a), we only use  $\|L^{-\top} \Lambda\| \leq \|L^{-\top} \gamma_{\max}\|$ . This can be seen from  $\|L^{-\top} \Lambda\| = \|\Lambda L^{-1}\|$  and  $L^{-\top} \Lambda \Lambda L^{-1} \leq \gamma_{\max}^2 L^{-\top} L^{-1}$ , where  $L^{-1}(\Lambda \Lambda^\top - \gamma_{\max}^2 \mathcal{I})L^{-\top} \leq 0$ . Thus,

$$\dot{\mathcal{W}}(u_{dq}, y) \leq \begin{bmatrix} \|u_{dq}\|_{\mathcal{S}'_u} \\ \|y\| \end{bmatrix}^\top \begin{bmatrix} -2(1-d)\xi_1 & -\frac{1}{2}(1-d)\beta_1 - \frac{1}{2}d\beta_2 \\ -\frac{1}{2}(1-d)\beta_1 - \frac{1}{2}d\beta_2 & d(\frac{\xi_2}{\varepsilon} - \zeta) \end{bmatrix} \begin{bmatrix} \|u_{dq}\|_{\mathcal{S}'_u} \\ \|y\| \end{bmatrix}.$$

By choosing  $\varepsilon$  in (14c) as explained in Ch.11.5 in [19], we note that the Lie derivative of  $\mathcal{W}$  is negative definite with respect to  $\mathcal{S}'$ .

The above arguments show that  $\mathcal{S}'$  is almost globally asymptotically stable for all trajectories of (13) and hence concludes the proof of Theorem IV.2.

**Remark 1.** We make the following remarks in order:

- 1) Note that the steady-state values of the voltage capacitor  $v_c^*$  are not necessarily required for the operation of the  $(\lambda - \omega)$  VOC. These can be readily obtained from the relationship  $v_{dq}^* = L^{-1}u_{dq}^*$ , where  $L = Z_G + \mathbf{B}Z_O^{-1}\mathbf{B}^\top$  and we can re-write the projector as  $\Pi_{dq} = \mathcal{I} - \frac{L^{-1}u_{dq}^* u_{dq}^{*\top} L^{-\top}}{u_{dq}^{*\top} L^{-1} u_{dq}^*}$ . Hence, the knowledge of only the desired current  $u_{dq}^*$  and the network parameters suffices to operate the  $(\lambda - \omega)$  VOC.
- 2) Our stability analysis implies that, when a frequency function  $\omega(\theta, \theta^*)$  is chosen as in (4), the control gain  $\alpha_k$  needs to be chosen to be sufficiently small as in Condition (14a). Example values are given later in Section V. Note that other variants of the frequency function can be selected, involving functions with feedback from available measurements either of the DC or AC sides.
- 3) The higher is the value of the line resistor  $R_O$ , the better condition (11) is satisfied. This corresponds to a small value of line inductance  $L_O$ . Typical values of the line inductance and line capacitance are around  $L_O = 7.66 \cdot 10^{-6} \text{H}$ ,  $C_O = 1.83 \cdot 10^{-8} \text{F}$ ,  $C = 10^{-5} \text{F}$  and their time constants correspond to  $5 \cdot 10^{-5}$  and  $10^{-6}$ , respectively, which shows a difference of at least one order of magnitude between them. This justifies Assumption 1 in practical scenarios.
- 4) Condition (14b) and (14c) depend on the steady states of the prescribed values of the input current/capacitor voltage and in particular on the desired voltage angles. They also depend on the network parameters, encoded in the impedance matrix  $L$ .
- 5) Condition (14c) is understood as a condition on the converter parameters. In particular, it verifies whether the resistive load with conductance  $G > G_{\min}$  satisfies (14c), where  $G_{\min}$  is the minimal acceptable load for which (14c) is fulfilled.

## V. SIMULATIONS

Our simulation setup consists of identical three-phase DC/AC converter model in closed-loop with the  $(\lambda - \omega)$  VOC as depicted in Figure 1 and connected via transmission lines according to  $\Pi$  model. The parameter values can be found in Table I.

We operate the converter initially at the desired steady state with currents and voltages values given by  $u_k^* = r_k^* [\cos(\theta_k^*) \sin(\theta_k^*)]$  with  $r_k^* = 20$  and  $\theta_k^* = 2\pi 50t + 1.1780$  with  $k = 1, 2, 3$  and corresponding output voltage of  $v_{c,k}^* = r_{c,k}^* [\cos(\theta_{c,k}^*) \sin(\theta_{c,k}^*)]$  with  $r_{c,k}^* = 175$  and  $\theta_c^* = 2\pi 50t - 2.463$ . We select all control gains and system parameters satisfying the sufficient stability conditions (14). We demonstrate the droop behavior of  $(\lambda - \omega)$  VOC as discussed in Proposition III.1 via an increase in power demand at

TABLE I  
PARAMETER VALUES OF THE THREE DC/AC CONVERTERS AND THE LINES (IN S.I.).

	$C_i, i = \{1,2,3\}$	RL Lines
$L$	$5 \cdot 10^{-4}$	–
$C$	$10^{-3}$	–
$G$	0.5	–
$R$	0.1	–
$C_O$	–	$10^{-8}$
$R_O$	–	0.2
$L_O$	–	$5 \cdot 10^{-5}$
$\gamma_{1,2,3}$	0.1	–
$\alpha_{1,2,3}$	0.03	–

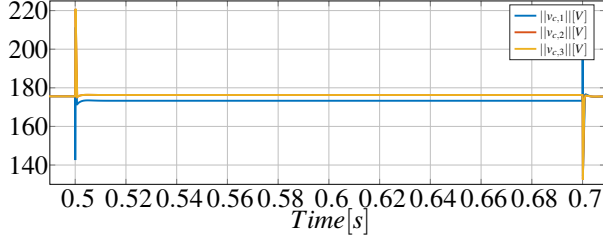


Fig. 4. Droop behavior in the amplitudes of the output voltages, at converters 1,2 and 3, as converter 1 experiences an increase in power demand. These correspond to the power profiles in Figure 5 .

converter 1. As shown in Figure 4, notice that an increase in the conductance value (modeling an increase in active power consumption) causes a drop in the amplitude of the output capacitor voltage at the affected converter (blue line). On the other hand, an increase in the voltage amplitude of the two other converters (red and yellow lines) compensate for the total increase in power demand. This can also be seen from the power profile of the three converters in Figure 5.

Finally, we vary the initial condition at one of the capacitor voltages  $v_{c1}(0)$  and plot the electromagnetic transients of the output capacitor voltage from different initial conditions. Even though our analysis considers a reduced-order model, the trajectories of (8) converge to their desired amplitude and phase angles, as shown in Figure 6.

## VI. CONCLUSION

We proposed a grid-forming control strategy inspired by wave phenomena in biological systems and building upon

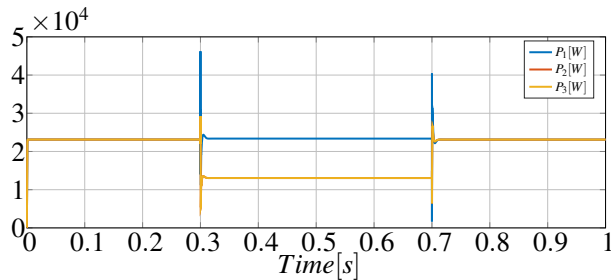


Fig. 5. Active power output of the converters 1, 2 and 3 following a step in the load conductance  $G$  of converter 1. Converters 2 and 3 provide power support.

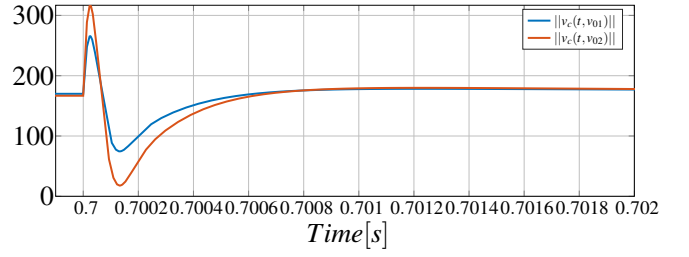


Fig. 6. Electromagnetic transients of the output voltage magnitude of converter 1 with two different initial conditions (after two different disturbances).

virtual oscillator control, while incrementing their dynamics with an adaptive frequency function. Our controller has droop behavior both in the amplitude and frequency. We proved almost global asymptotic stability of the desired set for a reduced-order model of converter network in closed-loop with  $(\lambda - \omega)$  VOC for a specified range of network parameters and control gains. We validated our results on a simulative three converter example. In our future work, we will consider a more detailed model of DC/AC converters and in particular include the DC-side dynamics in our analysis.

## APPENDIX

*Proof.* Let  $M_1(r) = \text{diag}\{\gamma_1 \begin{bmatrix} r_1^* & 0 \\ 0 & r_1^* \end{bmatrix}, \dots, \gamma_n \begin{bmatrix} r_n^* & 0 \\ 0 & r_n^* \end{bmatrix}\}$  and  $M_2(\theta) = \text{diag}\{\alpha_1 \begin{bmatrix} 0 & -(\theta_1 - \theta_1^*) \\ (\theta_1 - \theta_1^*) & 0 \end{bmatrix}, \dots, \alpha_n \begin{bmatrix} 0 & -(\theta_n - \theta_n^*) \\ (\theta_n - \theta_n^*) & 0 \end{bmatrix}\}$ . We calculate

$$\begin{aligned} & (\mathcal{I} - \frac{u_{dq}^* u_{dq}^{*\top}}{u_{dq}^{*\top} u_{dq}^*}) (M_1(r) + M_2(\theta)) \\ & + (M_1(r) + M_2(\theta))^\top (\mathcal{I} - \frac{u_{dq}^* u_{dq}^{*\top}}{u_{dq}^{*\top} u_{dq}^*}) = \\ & \underbrace{M_1(r) + M_1^\top(r) - (\frac{u_{dq}^* u_{dq}^{*\top}}{u_{dq}^{*\top} u_{dq}^*} M_1(r) + M_1^\top(r) \frac{u_{dq}^* u_{dq}^{*\top}}{u_{dq}^{*\top} u_{dq}^*})}_{D_{1,k}(\gamma_k)} \\ & + \underbrace{M_2(\theta) + M_2^\top(\theta) - (\frac{u_{dq}^* u_{dq}^{*\top}}{u_{dq}^{*\top} u_{dq}^*} M_2(\theta) + M_2^\top(\theta) \frac{u_{dq}^* u_{dq}^{*\top}}{u_{dq}^{*\top} u_{dq}^*})}_0. \end{aligned}$$

We calculate  $D_{1,k}(\gamma_k)$  as follows,

$$\begin{bmatrix} 2\gamma_k \frac{r_k^*}{r_k^*} - \frac{2r_k r_k^*}{\|u_{dq,k}^*\|^2} (\gamma_k s^2(\theta_k^*) r_k & - \frac{2r_k r_k^*}{\|u_{dq,k}^*\|^2} \gamma_k c(\theta_k^*) s(\theta_k^*) \\ - \frac{2r_k r_k^* \gamma_k}{\|u_{dq,k}^*\|^2} c(\theta_k^*) s(\theta_k^*) & 2\gamma_k \frac{r_k^*}{r_k^*} - \frac{2r_k r_k^*}{\|u_{dq,k}^*\|^2} (\gamma_k c^2(\theta_k^*) r_k) \end{bmatrix}$$

$$D_{2,k} = (\theta_k - \theta_k^*) \alpha_k r_k^* \begin{bmatrix} 2s(\theta_k^*) c(\theta_k^*) & (c(\theta_k^*) - s(\theta_k^*)) \\ (c(\theta_k^*) - s(\theta_k^*)) & -2s(\theta_k^*) c(\theta_k^*) \end{bmatrix}$$

where  $s(\cdot) = \sin(\cdot)$ ,  $c(\cdot) = \cos(\cdot)$  and  $u_{dq,k}^* = r_k^* [c(\theta_k^*) s(\theta_k^*)]^\top$ . This amounts to checking  $\text{diag}\{D_{1,1}(\gamma_1) - D_{2,1}, \dots, D_{1,n}(\gamma_n) - D_{2,n}\}$  for positive definiteness. Note that  $D_1(\gamma_k)$  is positive definite (by checking the trace and

determinant). Hence, for sufficiently small  $\alpha_k$ ,  $D_1(\gamma_k) - D_2$  is positive semi-definite. Since  $D_1(\gamma_{\max}) - D_{1,k}(\gamma_k)$  is positive definite with  $\gamma_{\max} = \max(\gamma_1, \dots, \gamma_n)$ , it follows that  $\Pi\Gamma + \Gamma\Pi \leq 2\gamma_{\max}\Pi$ .

□

## ACKNOWLEDGMENT

Taouba Jouini would like to thank Prof. Johannes Schiffer for the insightful comments and constructive discussions.

## REFERENCES

- [1] J. Machowski, J. Bialek, J. R. Bumby, and J. Bumby, *Power system dynamics and stability*. John Wiley & Sons, 1997.
- [2] M. Paolone, T. Gaunt, X. Guillaud, M. Liserre, S. Meliopoulos, A. Monti, T. Van Cutsem, V. Vittal, and C. Vournas, "Fundamentals of power systems modelling in the presence of converter-interfaced generation," *Electric Power Systems Research*, vol. 189, p. 106811, 2020.
- [3] J. W. Simpson-Porco, F. Dörfler, and F. Bullo, "Synchronization and power sharing for droop-controlled inverters in islanded microgrids," *Automatica*, vol. 49, no. 9, pp. 2603 – 2611, 2013.
- [4] H. Bevrani, T. Ise, and Y. Miura, "Virtual synchronous generators: A survey and new perspectives," *International Journal of Electrical Power & Energy Systems*, vol. 54, pp. 244–254, 2014.
- [5] C. Arghir, T. Jouini, and F. Dörfler, "Grid-forming control for power converters based on matching of synchronous machines," *Automatica*, vol. 95, pp. 273–282, 2018.
- [6] A. L. Fradkov and A. Y. Pogromsky, *Introduction to control of oscillations and chaos*. World Scientific, 1998, vol. 35.
- [7] B. B. Johnson, S. V. Dhople, A. O. Hamadeh, and P. T. Krein, "Synchronization of parallel single-phase inverters with virtual oscillator control," *IEEE Transactions on Power Electronics*, vol. 29, no. 11, pp. 6124–6138, 2014.
- [8] M. Colombino, D. Groß, J.-S. Brouillon, and F. Dörfler, "Global phase and magnitude synchronization of coupled oscillators with application to the control of grid-forming power inverters," *IEEE Transactions on Automatic Control*, vol. 64, no. 11, pp. 4496–4511, 2019.
- [9] M. Li, B. Wei, J. Matas, J. M. Guerrero, and J. C. Vasquez, "Advanced synchronization control for inverters parallel operation in microgrids using coupled hopf oscillators," *CPSS Transactions on Power Electronics and Applications*, vol. 5, no. 3, pp. 224–234, 2020.
- [10] M. Sinha, F. Dörfler, B. B. Johnson, and S. V. Dhople, "Virtual oscillator control subsumes droop control," in *2015 American Control Conference (ACC)*. IEEE, 2015, pp. 2353–2358.
- [11] J. D. Murray, *Mathematical biology: I. An introduction*. Springer Science & Business Media, 2007, vol. 17.
- [12] M.-S. Debyr, G. Denis, and T. Prevost, "Characterization of the grid-forming function of a power source based on its external frequency smoothing capability," in *2019 IEEE Milan PowerTech*. IEEE, 2019, pp. 1–6.
- [13] B. B. Johnson, S. V. Dhople, A. O. Hamadeh, and P. T. Krein, "Synchronization of parallel single-phase inverters with virtual oscillator control," *IEEE Transactions on Power Electronics*, vol. 29, no. 11, pp. 6124–6138, 2013.
- [14] M. Lu, S. Dutta, V. Purba, S. Dhople, and B. Johnson, "A grid-compatible virtual oscillator controller: Analysis and design," in *2019 IEEE Energy Conversion Congress and Exposition (ECCE)*. IEEE, 2019, pp. 2643–2649.
- [15] T. Jouini, C. Arghir, and F. Dörfler, "Grid-friendly matching of synchronous machines by tapping into the dc storage," *IFAC-PapersOnLine*, vol. 49, no. 22, pp. 192–197, 2016.
- [16] H. K. Khalil, *Nonlinear systems*, 3rd ed. Prentice hall New Jersey, 2002.
- [17] Y. Lin, E. D. Sontag, and Y. Wang, "A smooth converse lyapunov theorem for robust stability," *SIAM Journal on Control and Optimization*, vol. 34, no. 1, pp. 124–160, 1996.
- [18] D. Groß, M. Colombino, J.-S. Brouillon, and F. Dörfler, "The effect of transmission-line dynamics on grid-forming dispatchable virtual oscillator control," *IEEE Transactions on Control of Network Systems*, vol. 6, no. 3, pp. 1148–1160, 2019.
- [19] H. K. Khalil and J. W. Grizzle, *Nonlinear systems*. Prentice hall Upper Saddle River, NJ, 2002, vol. 3.
- [20] P. Monzón and R. Potrie, "Local and global aspects of almost global stability," in *45th IEEE Conference on Decision and Control*. IEEE, 2006, pp. 5120–5125.